SARS-CoV-2 RNAemia and proteomic biomarker trajectory inform prognostication in COVID-19 patients admitted to intensive care

Clemens Gutmann[1*], Kaloyan Takov[1*], Sean A. Burnap[1*], Bhawana Singh[1*], Konstantinos Theofilatos[1], Ella Reed[1], Maria Hasman[1], Adam Nabeebaccus[1,2], Matthew Fish,[3,4] Mark J.W. McPhail[2,5,6], Kevin O'Gallagher[1,2], Lukas E. Schmidt[1], Christian Cassel[1], Marieke Rienks[1], Xiaoke Yin[1], Georg Auzinger[2], Salvatore Napoli[5], Salma F. Mujib[6], Francesca Trovato[2,5,6], Barnaby Sanderson[4], Blair Merrick[7], Umar Niazi[8], Mansoor Saqi[8], Konstantina Dimitrakopoulou[8], Silke Braun[9], Romy Kronstein-Wiedemann[10], Katie J. Doores[3], Jonathan D. Edgeworth[3,7], Ajay M. Shah[1], Stefan R. Bornstein[11,12], Torsten Tonn[10,13], Adrian C. Hayday[3,14], Manu Shankar-Hari[3,4,15], Manuel Mayr[1,11,15].

[1] King's College London British Heart Foundation Centre, School of Cardiovascular Medicine and Sciences, London, UK.

[2] King's College Hospital NHS Foundation Trust, London, UK.

[3] Department of Infectious Diseases, School of Immunology and Microbial Sciences, King's College London, London, UK.

[4] Department of Intensive Care Medicine, Guy's and St Thomas' NHS Foundation Trust, London, UK.

[5] Department of Inflammation Biology, School of Immunology and Microbial Sciences, Faculty of Life Sciences and Medicine, King's College London, London, UK.

[6] Institute of Liver Studies, King's College Hospital, London, UK

[7] Clinical Infection and Diagnostics Research group, Department of Infection, Guy's and St Thomas' NHS Foundation Trust, London, UK

[8] NIHR Biomedical Research Centre, Guy's and St Thomas' NHS Foundation Trust and King's College London, London, UK

[9] Medical Clinic I, University Hospital Carl Gustav Carus, Technical University Dresden, Dresden, Germany

[10] Experimental Transfusion Medicine, Faculty of Medicine Carl Gustav Carus, Technical University Dresden, Dresden, Germany

[11] Department of Internal Medicine III, University Hospital Carl Gustav Carus, Technical University Dresden, Dresden, Germany

[12] Department of Diabetes, School of Life Course Science and Medicine, King's College London, London, UK

[13] Institute for Transfusion Medicine, German Red Cross Blood Donation Service North East, Dresden, Germany

[14] The Francis Crick Institute, London, UK

* Equal first author contribution.

Running title: SARS-CoV-2 RNAemia and Proteomics

[15] **To whom correspondence should be addressed:**

Dr. Manu Shankar-Hari; manu.shankar-hari@kcl.ac.uk or Prof. Manuel Mayr; King's British Heart Foundation Centre, King's College London, 125 Coldharbour Lane, London, SE59NU UK; Phone: +44(0)2078485446; +44(0)2078485298; manuel.mayr@kcl.ac.uk.

Abstract

Prognostic characteristics inform risk stratification in intensive care unit (ICU) patients with coronavirus disease 2019 (COVID-19). We obtained blood samples (*n* = 474) from hospitalized COVID-19 patients (*n* = 123), non-COVID-19 ICU sepsis patients (*n* = 25) and healthy controls (*n* = 30). Severe acute respiratory syndrome coronavirus 2 (SARS-CoV-2) RNA was detected in plasma or serum (RNAemia) of COVID-19 ICU patients when neutralizing antibody response was low. RNAemia was associated with higher 28-day ICU mortality (hazard ratio [HR], 1.84 [95% CI, 1.22–2.77] adjusted for age and sex). In longitudinal comparisons, COVID-19 ICU patients had a distinct proteomic trajectory associated with RNAemia and mortality. Among COVID-19-enriched proteins, galectin-3 binding protein (LGALS3BP) and proteins of the complement system were identified as interaction partners of SARS-CoV-2 spike glycoprotein. Finally, machine learning identified 'Age, RNAemia' and 'Age, pentraxin-3 (PTX3)' as the best binary signatures associated with 28-day ICU mortality.

Key Words: COVID-19 • SARS-CoV-2 • RNAemia • Pentraxin-3 • Biomarker • Proteomics

Introduction

Coronavirus disease 2019 (COVID-19) caused by the severe acute respiratory syndrome coronavirus 2 (SARS-CoV-2; a single-stranded RNA virus) poses an unprecedented challenge to health care systems globally. It is increasingly apparent that conventional prognostic scores for critically ill patients admitted to intensive care units (ICUs) such as the APACHE II (Acute Physiology and Chronic Health Evaluation) score[1] and SOFA (Sequential Organ Failure Assessment) score[2], are not discriminatory in COVID-19 ICU patients[3–6].

In this context, circulating SARS-CoV-2 RNA (RNAemia) has been highlighted as a promising prognostic biomarker in hospitalized COVID-19 patients, as it is associated with disease severity[7] and mortality[8–10], with an estimated prevalence of 10% (95% CI 5-18%, random effects model)[7]. Further, we hypothesized that the acute and profound alterations in the innate and adaptive immune system in COVID-19 patients[3,11–13], especially in RNAemic patients[14–18], will be accompanied by marked changes in the circulating proteome and interactome and that the proteome in COVID-19 patients will highlight mechanistically relevant signatures and trajectories, when compared to non-COVID-19 sepsis and healthy controls. Thus far, proteomics studies have focused on the determination of protein biomarkers of COVID-19 severity[19–22], but have not assessed the longitudinal relationship between proteomic changes, RNAemia and 28-day mortality.

In this study, we assessed RNAemia, antibody response against SARS-CoV-2 and proteomic profiles in serial blood samples from COVID-19 patients admitted to two ICUs. Controls included hospitalized, non-ICU COVID-19 patients as well as SARS-CoV-2-negative ICU sepsis and non-ICU patients. In the context of RNAemia, we explored the plasma protein interactions with the SARS-CoV-2 spike glycoprotein. Finally, we compared the associations of RNAemia and protein biomarkers with 28-day mortality, including established biomarkers

88 of acute respiratory distress syndrome (ARDS), *i.e.* receptor for advanced glycation end-
89 products (RAGE)[23–25], and prognosis in ICU patients with sepsis, *i.e.* pentraxin-3 (PTX3)[26–29].
90

91 **Results**

92 **Demographics and clinical characteristics of COVID-19 patients.** 474 blood samples were
93 available for analysis (Fig. 1, Supplementary Fig. 1): 295 longitudinal samples from ICU
94 patients with COVID-19 admitted to two university hospitals (GSTT; $n = 62$ and KCH; $n = 16$)
95 and samples from hospitalized, non-ICU COVID-19 patients for comparison ($n = 45$); ICU and
96 non-ICU patients without COVID-19 served as controls ($n = 55$). The baseline clinical
97 characteristics of all COVID-19 ICU patients are shown in Supplementary Table 1. The
98 primary outcome measure was defined as mortality 28 days after ICU admission. As
99 expected[30], non-survivors (23%) were older than survivors ($P = 0.0004$). COVID-19 patients
100 admitted to ICU were predominantly males (72%). All other characteristics, including common
101 comorbidities, the time from symptom onset to ICU admission, APACHE II score and SOFA
102 score, were similar between ICU survivors and non-survivors. The mortality rate in COVID-
103 19 ICU patients was twice as high as in hospitalized, non-ICU COVID-19 patients (23% *versus*
104 11%; Supplementary Table 2).
105

106 **Frequency of SARS-CoV-2 RNAemia and association with mortality in COVID-19 ICU**
107 **patients.** The presence of circulating viral RNA was analyzed by RT-qPCR. Serum (GSTT; n
108 $= 62$) and plasma (KCH; $n = 16$) samples were collected within 24 hours of admission to ICU
109 with COVID-19 and thereafter during week 1, week 2 and again before discharge. Since all 78
110 COVID-19 ICU patients were administered heparin and heparin has an inhibitory effect on
111 qPCR[31,32], RNA samples were treated with heparinase as previously described[33]. 18 of 78
112 (23%) COVID-19 ICU patients had detectable RNAemia within the first six days upon

113 admission to ICU (Supplementary Table 1). Strikingly, RNAemia within six days of admission
114 to ICU was detectable in 56% of non-survivors but only in 13% of survivors (P = 0.0006,
115 Supplementary Table 1). RNAemia was associated with a higher risk of 28-day mortality
116 (hazard ratio [HR], 2.05 [95% CI, 1.38–3.04]), that was comparable to age (2.89 [1.66-5.03],
117 Fig. 2a) and maintained after correction for age and sex (HR, 1.84 [95% CI, 1.22–2.77], Fig.
118 2b). In comparison, only 2 out of 45 (4%) non-ICU COVID-19 patients tested positive for
119 RNAemia upon hospitalization (Supplementary Table 2). General demographics and baseline
120 clinical characteristics of COVID-19 patients with and without RNAemia in the first six days
121 of admission to ICU are presented in Supplementary Table 3. Hypertension (r = 0.33, P =
122 0.003), type 2 diabetes (r = 0.24, P = 0.038), bilirubin (r = 0.32, P = 0.005), respiration rate (r
123 = 0.27, P = 0.018) and elevated potassium levels (r = 0.26, P = 0.023) were positively
124 correlated to RNAemia, whilst monocyte counts were inversely correlated (r = -0.23, P =
125 0.047, Fig. 2c). A hierarchical clustering analysis of all clinical variables and RNAemia is
126 presented in Supplementary Fig. 2. To confirm the specificity of our RT-qPCR assay, we
127 measured SARS-CoV-2 RNAemia in 134 plasma samples from 55 non-COVID-19 patients,
128 all of which tested negative (Supplementary Table 4 and 5).
129
130 **Humoral immune response during SARS-CoV-2 RNAemia.** In both COVID-19 ICU patient
131 cohorts, IgG antibodies to the SARS-CoV-2 spike S1 glycoprotein and SARS-CoV-2
132 neutralizing capacity were measured by ELISA and Surrogate Virus Neutralization Test,
133 respectively. The latter test evaluates the inhibition of binding of the receptor-binding domain
134 (RBD) of SARS-CoV-2 spike to ACE2. For validation, neutralization potency was correlated
135 to a HIV-1 based pseudotype neutralization assay in a subset of samples (38 samples from 16
136 ICU patients, r = 0.81, P <0.0001). COVID-19 ICU patients who tested positive or negative
137 for RNAemia within the first six days in ICU showed no difference in their strong IgG response

138 to SARS-CoV-2 S1 or in their neutralization capacity (Fig. 2d). However, when individual
139 samples were compared, RNAemia positive samples had lower anti-SARS-CoV-2 spike IgG
140 levels and lower SARS-CoV-2 neutralization capacity (Fig. 2e).
141
142 **Plasma proteome alterations in COVID-19 ICU patients.** To capture the host response of
143 COVID-19 ICU patients, we interrogated their plasma proteome. Baseline plasma samples
144 from COVID-19 ICU patients (KCH cohort, n = 12) were compared to COVID-19 negative
145 sepsis ICU patients (sepsis, n = 12) and patients prior to undergoing elective cardiac surgery
146 (controls, n = 30) (Supplementary Table 4 and 5). The plasma proteome was quantified by a
147 data-independent acquisition-mass spectrometry (DIA-MS) approach, using authentic heavy
148 peptide standards representing 500 proteins[34], revealing 100 significantly altered proteins
149 across the three patient groups ($q<0.05$) (Fig. 3a). Hierarchical cluster analysis highlighted a
150 cluster of 47 plasma proteins enriched in COVID-19, including members of the complement
151 cascade, as well as proteins involved in platelet degranulation, the acute phase response and
152 coagulation (Fig. 3a, b).
153 Of the 100 circulating proteins altered across control, sepsis ICU and COVID-19 ICU
154 patients, 29 overlapped with previous proteomic reports identifying markers of COVID-19
155 severity[19,20] (Supplementary Fig. 3). However, only few were associated with 28-day mortality,
156 as determined through DIA-MS analysis of baseline serum samples obtained from a larger
157 COVID-19 ICU patient cohort (GSTT, n = 62) (Fig. 3c). Complement factor B (CFB),
158 carboxypeptidase N (CPN1) and alpha-1-antichymotrypsin (SERPINA3) were all negatively
159 associated with outcome. An independent, publicly available dataset utilizing proximity-
160 extension assays (Olink, n = 264 survivors, n = 42 non-survivors, Supplementary Table 6) also
161 confirmed the lack of outcome association for three proteins identified as markers of COVID-

162 19 severity in previous proteomics studies[19,20]: lipopolysaccharide binding protein (LBP),
163 CD14, and inter-alpha-trypsin inhibitor heavy chain H3 (ITIH3) (Fig. 3c).
164 Protein changes that emerged as significantly associated with mortality in ICU patients
165 but have not been previously linked to the severity of COVID-19, included an elevation of
166 mannose binding lectin 2 (MBL2) and reductions in protein C (PROC), plasminogen (PLG)
167 and coagulation factor 7 (F7) (Fig. 3d). The associations of PROC and F7 with 28 days
168 mortality and the directionality of these associations were validated in the external validation
169 cohort mentioned above (Supplementary Table 6).
170
171 **Protein associations with SARS-CoV-2 RNAemia and clinical improvement.** Nine proteins
172 were significantly associated with RNAemia at baseline (GSTT COVID-19 ICU cohort) which
173 included an increase in plasma protease C1 inhibitor (SERPING1) and complement C4-A
174 (C4A); paralleled by a reduction in VE-cadherin (CDH5) and complement factor H-related
175 protein 1 (CFHR1) (Fig. 4a). In longitudinal serum samples from the GSTT cohort (baseline,
176 week 1 and week 2; $n = 47$), a greater increase of polymeric immunoglobulin receptor (PIGR)
177 was observed in RNAemia positive, compared to RNAemia negative ICU patients (Fig. 4b).
178 In contrast, kallikrein (KLKB1) levels significantly increased over time but tended to be higher
179 in RNAemia negative ICU patients (Fig. 4b).
180 Hierarchical cluster analysis upon significantly changing serum proteins over the two-
181 week period (baseline, week 1 and week 2) revealed four distinct protein clusters (Fig. 4c),
182 which were annotated by gene ontology enrichment analysis. Alterations in PIGR correlated
183 closely with neutrophil degranulation proteins such as S100A8 and S100A9 (Fig. 4c, Cluster
184 2), while KLKB1 kinetics followed members of the coagulation system (Fig. 4c, Cluster 4). A
185 comparison of the trajectories of individual proteins between patients who survived and died
186 is shown in Supplementary Fig. 4. The most pronounced changes were observed among

187 proteins constituting cluster 4, with recovery of liver-derived proteins linked to lipid
188 metabolism and coagulation being significantly suppressed in patients who died (Fig. 4c).
189
190 **LGALS3BP is enriched in COVID-19 and binds to SARS-CoV-2 spike glycoprotein.** The
191 spike glycoprotein is the largest protein in the viral envelope, responsible for cell entry and is
192 the main target of neutralizing antibodies[35]. A magnetic affinity pull-down of a His-tagged
193 SARS-CoV-2 spike glycoprotein mixed with plasma from COVID-19 ICU patients was
194 coupled with proteomics to determine interaction partners. Proteomic analysis identified 32
195 spike-binding proteins. A large proportion were immunoglobulins (Fig. 5a) and members of
196 the complement system, which are known to directly interact with antigen-bound antibodies
197 (*i.e.* C1 complement complex, Fig. 5b, Supplementary Table 7). Additional interaction partners
198 included complement component 4 binding proteins alpha and beta (C4BPA and C4BPB),
199 CPN1 (among the proteins associated with 28-day mortality) and galectin-3-binding protein
200 (LGALS3BP). Apart from apolipoprotein D (APOD), LGALS3BP was the only protein to be
201 retrieved to a greater extent with spike glycoprotein from plasma of COVID-19 ICU patients
202 compared to pre-pandemic sepsis ICU patients (Fig. 5c, Supplementary Table 8).
203 LGALS3BP was markedly elevated in COVID-19 patients as discovered by DIA-MS
204 and confirmed by ELISA, but unchanged between control and sepsis patients without COVID-
205 19 (Fig. 5d). Strikingly, LGALS3BP was among the most elevated proteins when compared to
206 sepsis ICU patients (Fig. 5e). Of the proteins revealed to bind spike, only LGALS3BP and
207 members of the complement cascade were also specifically elevated in COVID-19 ICU
208 patients. LGALS3BP revealed a strong positive correlation with members of the complement
209 cascade (C6, C9, C4BPA and C4BPB) and CPN1, but a negative correlation with adiponectin
210 (ADIPOQ) (Fig. 5f). LGALS3BP abundance in COVID-19 patients closely correlated with

211 regulators of the complement cascade, platelet degranulation and the innate immune system
212 (Fig. 5f, Supplementary Fig. 5).
213
214 **SARS-CoV-2 mortality prediction using machine learning.** RAGE is an established
215 biomarker of ARDS[23–25], but remained unaffected by SARS-CoV-2 RNAemia and mortality
216 (Supplementary Fig. 6a). PTX3, however, a protein we and others have previously highlighted
217 as a prognostic marker in ICU patients with sepsis[26–29], positively associated with COVID-19
218 mortality (Supplementary Fig. 6b). Notably, PTX3 emerged as one of the best predictors for
219 mortality among 1,526 proteins measured in the external validation cohort of hospitalized
220 COVID-19 patients described above (n = 264 survivors; n = 42 non-survivors), outperforming
221 all measured cytokines and chemokines (Supplementary Table 6). Thus, a machine learning-
222 based approach was adopted to determine the best binary combination of clinical variables,
223 RNAemia and protein biomarkers that are independently associated with 28-day COVID-19
224 mortality. Kaplan Meier plots highlight RNAemia (P <0.0001) as the best individual predictor
225 (Fig. 6a-c, Supplementary Table 9), while the binary combinations 'Age, RNAemia' (P
226 <0.0001) and 'Age, PTX3' (P <0.0001), improved sensitivity compared to single markers, and
227 provided better survival stratification (Fig. 6d-f, Supplementary Table 9).
228
229 **Discussion**
230 To the best of our knowledge, this is the largest longitudinal assessment of RNAemia,
231 humoral immune response against SARS-CoV-2, protein biomarkers and clinical variables in
232 COVID-19 ICU patients to date. SARS-CoV-2 RNAemia was observed in 23% of COVID-19
233 ICU patients within the first six days of admission to ICU, which is more frequent than its
234 estimated prevalence (10% [95% CI 5-18%], random effects model)[7]. Likely explanations
235 include the fact that RNAemia is expected to be more common in ICU patients due to disease

236 severity[7]. Second, we optimized detection by treating isolated RNA with heparinase[33] to
237 overcome the known inhibitory effect of heparin on qPCR[31,32]. We also performed a two-step
238 RT-qPCR protocol rather than the one-step RT-qPCR protocol used in clinical practice and
239 previous studies in which RNAemia has been assessed thus far. Third, RNAemia was more
240 frequent closer to the onset of symptoms[7] and when humoral response against SARS-CoV-2
241 was low. The latter observation was maintained after correcting for time since onset of
242 symptoms. Thus, this is not a mere reflection of low humoral response in early sampling points.

243 RNAemia within six days of ICU admission was strongly associated with 28-day
244 mortality, which is a well-defined clinical outcome measure[36] also suitable for COVID-19 ICU
245 patients[5]. Thus far, studies on RNAemia included predominantly non-ICU patients and
246 associated RNAemia with disease severity[7]. Few studies also reported on the ability of
247 RNAemia to predict mortality[8–10] but none of these studies specifically focused on ICU patients
248 in which RNAemia is likely to be most informative. In our study, RNAemia was more frequent
249 in ICU patients with type 2 diabetes and hypertension, two well-known risk factors for poor
250 outcome in COVID-19. Using droplet digital PCR[15], RNAemia might become even more
251 frequent but the clinical relevance of very low levels of RNAemia is unclear. In comparison to
252 RNAemia as assessed in our study (HR, 1.84 [95% CI, 1.22–2.77] adjusted for age and sex),
253 the mortality risk conferred by increased nasopharyngeal SARS-CoV-2 RNA abundance was
254 found to be small (HR, 1.07 [95% CI, 1.03–1.11], n = 1,145)[37].

255 RNAemia could be a consequence of severe disease or might contribute to poor
256 outcome. Given that the SARS-CoV-2 entry receptor ACE2 is expressed on vascular cells,
257 including endothelial cells, smooth muscle cells and pericytes of most organs[38,39], and SARS-
258 CoV-2 RNA was detected in lungs, pharynx, heart, liver, brain and kidneys of autopsy tissue[40],
259 RNAemia could reflect the extent of viral dissemination. Notably, serum levels of CDH5, an
260 endothelial specific surface protein, differed between RNAemia positive *versus* negative ICU

261 patients. RNAemia was also inversely associated with monocyte counts. A decrease in
262 monocyte counts in COVID-19 patients has been attributed to extravasation and recruitment to
263 lungs[11,41].

264 Strikingly, patients with RNAemia showed dysregulation in several components of the
265 complement, the coagulation and the kinin-kallikrein system. Viral envelope glycoproteins are
266 an important trigger of the contact activation system[42] leading to a combined activation of these
267 pathways, a hallmark of thromboinflammation[42]. SARS-CoV spike is a ligand of MBL2[43,44] -
268 a pattern recognition molecule that initiates the lectin complement pathway[45]. Additionally,
269 high levels of MBL2 are known to increase lectin pathway-mediated tissue damage[46,47]. This
270 is consistent with our observation of a higher risk of mortality in COVID-19 ICU patients with
271 elevated MBL2 levels. Systemic complement activation has been associated with respiratory
272 failure in hospitalized COVID-19 patients[48] and complement deficiencies have been reported
273 to have protective effects on COVID-19-associated morbidity and mortality[49]. Besides
274 KLKB1, PIGR showed a different trajectory in RNAemia positive ICU patients. PIGR is a
275 receptor that transports polymeric IgA and IgM from the basolateral to the apical surface of
276 airway and gut mucosal cells[50]. Apart from its protective role, PIGR can be used by pathogens
277 such as *Streptococcus pneumoniae* to facilitate infection of airway epithelial cells[51] and its
278 plasma and lung tissue levels have been associated with severity of idiopathic pulmonary
279 fibrosis[52], and cystic fibrosis[53], respectively.

280 Pull-down experiments using SARS-CoV-2 spike glycoprotein returned several
281 members of the complement system. The complement system recruits neutrophils (C3a and
282 C5a[54]), is essential for neutrophil extracellular trap (NET) formation (C3[55] and C3aR[56]), and
283 can trigger NET formation (C5a[57]) when neutrophils are primed by interferon alpha or
284 gamma[57] – cytokines that we previously found elevated in severe COVID-19 patients[11].
285 Furthermore, binding of C1q to NETs protects NETs from degradation by DNases in the

286 circulation[58]. NETosis was previously shown to be promoted by SARS-CoV-2 RNAemia but
287 the mechanism remained elusive[16]. NET formation is also a prothrombotic process[59], and
288 thrombotic complications are highly prevalent in severe COVID-19[60]. NET formation itself is
289 part of a positive feedback loop, leading to activation of the alternative pathway of
290 complement[61], the contact activation system[62], kinin-kallikrein system[62] and release of
291 neutrophil-derived proteins, including the humoral pattern recognition receptor PTX3[63]. PTX3
292 is important for activation (through MBL2 and C1q)[64] and regulation (through CFH and
293 C4BPB)[65,66] of the complement system[67]. It is noteworthy that PTX3 has been validated as one
294 of the best predictors for mortality in an independent cohort of hospitalized COVID-9 patients
295 covering 1,526 plasma proteins (Supplementary Table 6, https://www.olink.com/mgh-covid-
296 study/).

297 Besides members of the complement system, we demonstrate that LGALS3BP is a
298 novel putative binding partner of SARS-CoV-2 spike glycoprotein. LGALS3BP is prominently
299 expressed in the lung[68] and possesses antiviral activity[69]. The rise in circulating LGALS3BP is
300 not observed in non-COVID-19 sepsis ICU patients, highlighting the specificity for viral over
301 bacterial infections. LGALS3BP directly interacts with adeno-associated viruses, inducing
302 viral particle aggregation and an impairment of transduction[70]. Similarly, LGALS3BP reduces
303 the infectivity of human immunodeficiency virus particles[71]. It is currently unknown if
304 LGALS3BP-spike binding also affects the infectivity of SARS-CoV-2, *i.e.* by competing with
305 binding to ACE2 or preventing the subsequent spike cleavage, which is essential for viral
306 entry[72]. Additionally, the direct interaction between LGALS3BP and SARS-CoV-2 spike
307 remains to be confirmed. Pull-down assays cannot rule out indirect binding to the bait protein.

308 In summary, RNAemia is frequent in COVID-19 ICU patients and associated with a
309 higher risk of mortality. To our knowledge, SARS-CoV-2 RNA is the only disease-specific
310 biomarker that has been associated with COVID-19 severity and mortality to date. Patients

311 with RNAemia may benefit from personalized treatment options. Finally, proteomic analyses
312 of blood samples from ICU patients with COVID-19 uncovered protein trajectories that
313 associated with RNAemia status, predicted 28-day mortality and identified LGALS3BP as a
314 novel interaction partner of the SARS-CoV-2 spike glycoprotein. Further studies are required
315 to assess the role of complement activation in COVID-19 on outcomes and explore the effect
316 of LGALS3BP on the infectivity of SARS-CoV-2.
317

References

1. Knaus, W. A., Draper, E. A., Wagner, D. P. & Zimmerman, J. E. APACHE II: a severity of disease classification system. *Crit. Care Med.* **13**, 818–29 (1985).
2. Vincent, J. L. *et al.* The SOFA (Sepsis-related Organ Failure Assessment) score to describe organ dysfunction/failure. On behalf of the Working Group on Sepsis-Related Problems of the European Society of Intensive Care Medicine. *Intensive Care Med.* **22**, 707–10 (1996).
3. Sinha, P. *et al.* Prevalence of phenotypes of acute respiratory distress syndrome in critically ill patients with COVID-19: a prospective observational study. *Lancet. Respir. Med.* **0**, (2020).
4. Zou, X. *et al.* Acute Physiology and Chronic Health Evaluation II Score as a Predictor of Hospital Mortality in Patients of Coronavirus Disease 2019. *Crit. Care Med.* **48**, e657–e665 (2020).
5. Intensive Care National Audit And Research Centre. *ICNARC report on COVID-19 in critical care 31 July 2020*. (2020).
6. Gupta, R. K. *et al.* Systematic evaluation and external validation of 22 prognostic models among hospitalised adults with COVID-19: An observational cohort study. *Eur. Respir. J.* (2020). doi:10.1183/13993003.03498-2020
7. Andersson, M. I. *et al.* SARS-CoV-2 RNA detected in blood products from patients with COVID-19 is not associated with infectious virus. *Wellcome Open Res.* **5**, 181 (2020).
8. Xu, D. *et al.* Relationship Between serum SARS-CoV-2 nucleic acid(RNAemia) and Organ Damage in COVID-19 Patients: A Cohort Study. *Clin. Infect. Dis.* (2020). doi:10.1093/cid/ciaa1085
9. Fajnzylber, J. M. *et al.* SARS-CoV-2 Viral Load is Associated with Increased Disease Severity and Mortality. *medRxiv* 2020.07.15.20131789 (2020). doi:10.1101/2020.07.15.20131789
10. Prebensen, C. *et al.* Severe Acute Respiratory Syndrome Coronavirus 2 RNA in Plasma Is Associated With Intensive Care Unit Admission and Mortality in Patients Hospitalized With Coronavirus Disease 2019. *Clin. Infect. Dis.* (2020). doi:10.1093/cid/ciaa1338
11. Laing, A. G. *et al.* A dynamic COVID-19 immune signature includes associations with poor prognosis. *Nat. Med.* 1–13 (2020). doi:10.1038/s41591-020-1038-6
12. Carter, M. J. *et al.* Peripheral immunophenotypes in children with multisystem inflammatory syndrome associated with SARS-CoV-2 infection. *Nat. Med.* 1–7 (2020). doi:10.1038/s41591-020-1054-6
13. Seow, J. *et al.* Longitudinal observation and decline of neutralizing antibody responses in the three months following SARS-CoV-2 infection in humans. *Nat. Microbiol.* 1–10 (2020). doi:10.1038/s41564-020-00813-8
14. Chen, X. *et al.* Detectable Serum Severe Acute Respiratory Syndrome Coronavirus 2 Viral Load (RNAemia) Is Closely Correlated With Drastically Elevated Interleukin 6 Level in Critically Ill Patients With Coronavirus Disease 2019. *Clin. Infect. Dis.* (2020). doi:10.1093/cid/ciaa449
15. Bermejo-Martin, J. F. *et al.* Viral RNA load in plasma is associated with critical illness and a dysregulated host response in COVID-19. *medRxiv* 2020.08.25.20154252 (2020). doi:10.1101/2020.08.25.20154252
16. Veras, F. P. *et al.* SARS-CoV-2–triggered neutrophil extracellular traps mediate COVID-19 pathology. *J. Exp. Med.* **217**, (2020).
17. Zaid, Y. *et al.* Platelets Can Associate with SARS-Cov-2 RNA and Are

367 Hyperactivated in COVID-19. *Circ. Res.* CIRCRESAHA.120.317703 (2020).
368 doi:10.1161/CIRCRESAHA.120.317703
369 18. Zhang, S. *et al.* SARS-CoV-2 binds platelet ACE2 to enhance thrombosis in COVID-
370 19. *J. Hematol. Oncol.* **13**, 120 (2020).
371 19. Shen, B. *et al.* Proteomic and Metabolomic Characterization of COVID-19 Patient
372 Sera. *Cell* **182**, 59-72.e15 (2020).
373 20. Messner, C. B. *et al.* Ultra-High-Throughput Clinical Proteomics Reveals Classifiers
374 of COVID-19 Infection. *Cell Syst.* **11**, 11-24.e4 (2020).
375 21. Overmyer, K. A. *et al.* Large-Scale Multi-omic Analysis of COVID-19 Severity. *Cell*
376 *Syst.* (2020). doi:10.1016/J.CELS.2020.10.003
377 22. Di, B. *et al.* Identification and validation of predictive factors for progression to severe
378 COVID-19 pneumonia by proteomics. *Signal Transduct. Target. Ther.* **5**, 217 (2020).
379 23. Jones, T. K. *et al.* Plasma sRAGE Acts as a Genetically Regulated Causal Intermediate
380 in Sepsis-associated Acute Respiratory Distress Syndrome. *Am. J. Respir. Crit. Care*
381 *Med.* **201**, 47–56 (2020).
382 24. Jabaudon, M. *et al.* Plasma sRAGE is independently associated with increased
383 mortality in ARDS: a meta-analysis of individual patient data. *Intensive Care Med.* **44**,
384 1388–1399 (2018).
385 25. Jabaudon, M. *et al.* Soluble form of the receptor for advanced glycation end products
386 is a marker of acute lung injury but not of severe sepsis in critically ill patients. *Crit.*
387 *Care Med.* **39**, 480–8 (2011).
388 26. Cuello, F. *et al.* Redox state of pentraxin 3 as a novel biomarker for resolution of
389 inflammation and survival in sepsis. *Mol. Cell. Proteomics* **13**, 2545–57 (2014).
390 27. Mauri, T. *et al.* Persisting high levels of plasma pentraxin 3 over the first days after
391 severe sepsis and septic shock onset are associated with mortality. *Intensive Care Med.*
392 **36**, 621–629 (2010).
393 28. Muller, B. *et al.* Circulating levels of the long pentraxin PTX3 correlate with severity
394 of infection in critically ill patients. *Crit. Care Med.* **29**, 1404–7 (2001).
395 29. Porte, R. *et al.* The Long Pentraxin PTX3 as a Humoral Innate Immunity Functional
396 Player and Biomarker of Infections and Sepsis. *Front. Immunol.* **10**, 794 (2019).
397 30. Williamson, E. J. *et al.* Factors associated with COVID-19-related death using
398 OpenSAFELY. *Nature* 1–7 (2020). doi:10.1038/s41586-020-2521-4
399 31. Ding, M. *et al.* An optimized sensitive method for quantitation of DNA/RNA viruses
400 in heparinized and cyropreserved plasma. *J. Virol. Methods* **176**, 1–8 (2011).
401 32. Kaudewitz, D. *et al.* Impact of intravenous heparin on quantification of circulating
402 microRNAs in patients with coronary artery disease. *Thromb. Haemost.* **110**, 609–615
403 (2013).
404 33. Schulte, C. *et al.* Comparative Analysis of Circulating Noncoding RNAs Versus
405 Protein Biomarkers in the Detection of Myocardial Injury. *Circ. Res.* **125**, 328–340
406 (2019).
407 34. Dupuis, N., Muller, S., Treiber, T. & Escher, C. Evaluation of PQ500, a 500-plasma
408 protein blood panel in NSCLC subjects using high-throughput MRM mass
409 spectrometry. *J. Clin. Oncol.* **37**, 110–110 (2019).
410 35. Ou, X. *et al.* Characterization of spike glycoprotein of SARS-CoV-2 on virus entry
411 and its immune cross-reactivity with SARS-CoV. *Nat. Commun.* **11**, 1620 (2020).
412 36. Vincent, J.-L. Endpoints in sepsis trials: More than just 28-day mortality? *Crit. Care*
413 *Med.* **32**, S209–S213 (2004).
414 37. Pujadas, E. *et al.* SARS-CoV-2 viral load predicts COVID-19 mortality. *Lancet*
415 *Respir. Med.* **0**, (2020).
416 38. Cardot-Leccia, N., Hubiche, T., Dellamonica, J., Burel-Vandenbos, F. & Passeron, T.

Pericyte alteration sheds light on micro-vasculopathy in COVID-19 infection. *Intensive Care Med.* **46**, 1777–1778 (2020).
39. Hamming, I. *et al.* Tissue distribution of ACE2 protein, the functional receptor for SARS coronavirus. A first step in understanding SARS pathogenesis. *J. Pathol.* **203**, 631 (2004).
40. Puelles, V. G. *et al.* Multiorgan and Renal Tropism of SARS-CoV-2. *N. Engl. J. Med.* **383**, 590–592 (2020).
41. Sánchez-Cerrillo, I. *et al.* COVID-19 severity associates with pulmonary redistribution of CD1c+ DC and inflammatory transitional and nonclassical monocytes. *J. Clin. Invest.* (2020). doi:10.1172/JCI140335
42. Risitano, A. M. *et al.* Complement as a target in COVID-19? *Nat. Rev. Immunol.* **20**, 343–344 (2020).
43. Zhou, Y. *et al.* A single asparagine-linked glycosylation site of the severe acute respiratory syndrome coronavirus spike glycoprotein facilitates inhibition by mannose-binding lectin through multiple mechanisms. *J. Virol.* **84**, 8753–64 (2010).
44. Ip, W. K. E. *et al.* Mannose-binding lectin in severe acute respiratory syndrome coronavirus infection. *J. Infect. Dis.* **191**, 1697–704 (2005).
45. Degn, S. E. *et al.* Complement activation by ligand-driven juxtaposition of discrete pattern recognition complexes. *Proc. Natl. Acad. Sci. U. S. A.* **111**, 13445–50 (2014).
46. Jordan, J. E., Montalto, M. C. & Stahl, G. L. Inhibition of Mannose-Binding Lectin Reduces Postischemic Myocardial Reperfusion Injury. *Circulation* **104**, 1413–1418 (2001).
47. Schafranski, M. D., Stier, A., Nisihara, R. & Messias-Reason, I. J. T. Significantly increased levels of mannose-binding lectin (MBL) in rheumatic heart disease: a beneficial role for MBL deficiency. *Clin. Exp. Immunol.* **138**, 521–5 (2004).
48. Holter, J. C. *et al.* Systemic complement activation is associated with respiratory failure in COVID-19 hospitalized patients. *Proc. Natl. Acad. Sci. U. S. A.* **117**, 25018–25025 (2020).
49. Ramlall, V. *et al.* Immune complement and coagulation dysfunction in adverse outcomes of SARS-CoV-2 infection. *Nat. Med.* 1–7 (2020). doi:10.1038/s41591-020-1021-2
50. Li, Y. *et al.* Structural insights into immunoglobulin M. *Science* **367**, 1014–1017 (2020).
51. Zhang, J.-R. *et al.* The Polymeric Immunoglobulin Receptor Translocates Pneumococci across Human Nasopharyngeal Epithelial Cells. *Cell* **102**, 827–837 (2000).
52. Todd, J. L. *et al.* Peripheral blood proteomic profiling of idiopathic pulmonary fibrosis biomarkers in the multicentre IPF-PRO Registry. *Respir. Res.* **20**, 227 (2019).
53. Collin, A. M. *et al.* Lung immunoglobulin A immunity dysregulation in cystic fibrosis. *EBioMedicine* **60**, 102974 (2020).
54. Haas, P.-J. & van Strijp, J. Anaphylatoxins: their role in bacterial infection and inflammation. *Immunol. Res.* **37**, 161–75 (2007).
55. Yipp, B. G. *et al.* Infection-induced NETosis is a dynamic process involving neutrophil multitasking in vivo. *Nat. Med.* **18**, 1386–93 (2012).
56. Guglietta, S. *et al.* Coagulation induced by C3aR-dependent NETosis drives protumorigenic neutrophils during small intestinal tumorigenesis. *Nat. Commun.* **7**, 11037 (2016).
57. Martinelli, S. *et al.* Induction of genes mediating interferon-dependent extracellular trap formation during neutrophil differentiation. *J. Biol. Chem.* **279**, 44123–32 (2004).
58. Leffler, J. *et al.* Neutrophil extracellular traps that are not degraded in systemic lupus

erythematosus activate complement exacerbating the disease. *J. Immunol.* **188**, 3522–31 (2012).
59. Kimball, A. S., Obi, A. T., Diaz, J. A. & Henke, P. K. The Emerging Role of NETs in Venous Thrombosis and Immunothrombosis. *Front. Immunol.* **7**, 236 (2016).
60. Zhang, L. *et al.* Deep Vein Thrombosis in Hospitalized Patients With COVID-19 in Wuhan, China: Prevalence, Risk Factors, and Outcome. *Circulation* **142**, 114–128 (2020).
61. Wang, H., Wang, C., Zhao, M.-H. & Chen, M. Neutrophil extracellular traps can activate alternative complement pathways. *Clin. Exp. Immunol.* **181**, 518–27 (2015).
62. Oehmcke, S., Mörgelin, M. & Herwald, H. Activation of the human contact system on neutrophil extracellular traps. *J. Innate Immun.* **1**, 225–30 (2009).
63. Jaillon, S. *et al.* The humoral pattern recognition receptor PTX3 is stored in neutrophil granules and localizes in extracellular traps. *J. Exp. Med.* **204**, 793–804 (2007).
64. Ma, Y. J. *et al.* Heterocomplexes of mannose-binding lectin and the pentraxins PTX3 or serum amyloid P component trigger cross-activation of the complement system. *J. Biol. Chem.* **286**, 3405–17 (2011).
65. Deban, L. *et al.* Binding of the long pentraxin PTX3 to factor H: interacting domains and function in the regulation of complement activation. *J. Immunol.* **181**, 8433–40 (2008).
66. Braunschweig, A. & Józsi, M. Human Pentraxin 3 Binds to the Complement Regulator C4b-Binding Protein. *PLoS One* **6**, e23991 (2011).
67. Ma, Y. J. & Garred, P. Pentraxins in Complement Activation and Regulation. *Front. Immunol.* **9**, 3046 (2018).
68. Ullrich, A. *et al.* The secreted tumor-associated antigen 90K is a potent immune stimulator. *J. Biol. Chem.* **269**, 18401–7 (1994).
69. Loimaranta, V., Hepojoki, J., Laaksoaho, O. & Pulliainen, A. T. Galectin-3-binding protein: A multitask glycoprotein with innate immunity functions in viral and bacterial infections. *J. Leukoc. Biol.* **104**, 777–786 (2018).
70. Denard, J. *et al.* Human galectin 3 binding protein interacts with recombinant adeno-associated virus type 6. *J. Virol.* **86**, 6620–31 (2012).
71. Wang, Q., Zhang, X., Han, Y., Wang, X. & Gao, G. M2BP inhibits HIV-1 virion production in a vimentin filaments-dependent manner. *Sci. Rep.* **6**, 32736 (2016).
72. Hoffmann, M. *et al.* SARS-CoV-2 Cell Entry Depends on ACE2 and TMPRSS2 and Is Blocked by a Clinically Proven Protease Inhibitor. *Cell* **181**, 271-280.e8 (2020).
73. Vogels, C. B. F. *et al.* Analytical sensitivity and efficiency comparisons of SARS-CoV-2 RT–qPCR primer–probe sets. *Nat. Microbiol.* 1–7 (2020). doi:10.1038/s41564-020-0761-6
74. Troyanskaya, O. *et al.* Missing value estimation methods for DNA microarrays. *Bioinformatics* **17**, 520–525 (2001).
75. Saeys, Y., Inza, I. & Larranaga, P. A review of feature selection techniques in bioinformatics. *Bioinformatics* **23**, 2507–2517 (2007).
76. Cortes, C. & Vapnik, V. Support-vector networks. *Mach. Learn.* **20**, 273–297 (1995).
77. Chawla, N. V., Bowyer, K. W., Hall, L. O. & Kegelmeyer, W. P. SMOTE: Synthetic Minority Over-sampling Technique. *J. Artif. Intell. Res.* **16**, 321–357 (2002).
78. Pedregosa, F. *et al.* Scikit-learn: Machine Learning in Python. *J. Mach. Learn. Res.* **12**, 2825–30 (2011).
79. Ojala, M. & Garrica, G. C. Permutation Tests for Studying Classifier Performance. *J. Mach. Learn. Res.* **11**, 1833–1863 (2010).
80. Kornbrot, D. Point Biserial Correlation. in *Encyclopedia of Statistics in Behavioral Science* (John Wiley & Sons, Ltd, 2005). doi:10.1002/0470013192.bsa485

517 **Methods**
518
519 **Study design and recruitment.** An overview of the study design is presented in
520 Supplementary Fig. 1. *COVID-19 cohorts.* COVID-19-positive patients, as confirmed by RT-
521 qPCR of nasopharyngeal samples, who were admitted to the ICUs of Guy's and St Thomas'
522 NHS Foundation Trust (GSTT) and King's College Hospital (KCH) between March 12, 2020
523 and July 1, 2020, were recruited for an observational cohort study with serial blood sampling
524 and analysis of clinical outcomes. The primary outcome measure was defined as mortality 28
525 days after ICU admission. Serial blood sampling was performed within 24 hours of admission
526 to ICU and thereafter three measurements were taken during week 1, week 2 and again before
527 discharge. In addition, we obtained plasma samples from COVID-19 patients upon
528 hospitalization at GSTT (non-ICU COVID-19 cohort). *Non-COVID-19 comparator cohorts.*
529 Plasma was collected from patients enrolled at the same time in the same KCH ICU as our
530 COVID-19 ICU cohort but who repeatedly tested negative for nasopharyngeal SARS-CoV-2
531 (intra-pandemic, non-COVID-19 ICU cohort). Serial blood sampling of these samples was
532 performed identical to our COVID-19 cohort. Additionally, pre-pandemic plasma samples
533 from patients recruited at GSTT prior to the COVID-19 pandemic were available as controls.
534 This included serial plasma samples from sepsis ICU patients (pre-pandemic, non-COVID-19
535 ICU sepsis cohort), collected upon admission and at three timepoints thereafter; as well as
536 plasma samples from patients before elective cardiac surgery (pre-pandemic, non-COVID-19
537 control cohort). The study was approved by an institutional review board (REC19/NW/0750
538 for all patients recruited at KCH; REC19/SC/0187 for patients recruited at GSTT of the
539 COVID-19 ICU cohort, the pre-pandemic sepsis ICU cohort, the pre-pandemic control cohort;
540 REC19/SC/0232 for patients recruited at GSTT of the non-ICU COVID-19 cohort). Written
541 informed consent was obtained directly from patients (if mentally competent), or from the next

542 of kin or professional consultee. The consent procedure was then completed with retrospective
543 consent if the patient regained capacity.
544
545 **Inactivation of serum and plasma**. Plasma was collected in EDTA BD Vacutainer™ tubes
546 (BD, 362799), whereas serum was collected in silica BD Vacutainer™ tubes (BD, 367820)
547 and left to clot for 15 min. Plasma and serum tubes were then centrifuged at 2,000 x g for 15
548 min. Infectious samples were then transferred to a containment level 3 facility for safe
549 inactivation. Samples destined for RNA extraction were inactivated by addition of 100 µL of
550 serum or plasma to 500 µL QIAzol (Qiagen, 79306), followed by 40 s of vortexing and 5 min
551 incubation at room temperature. Samples destined for protein analysis were inactivated by
552 addition of 1% (v/v) Triton X-100 (Sigma, T8787) and 1% (v/v) tributyl phosphate (Sigma,
553 00675), followed by 15 s of vortexing and 4 h incubation at room temperature. All samples
554 were then frozen at -80°C until further processing.
555
556 **RNA extraction and heparinase treatment.** Total RNA was extracted using the miRNeasy
557 Mini kit (Qiagen, 217004) according to the manufacturer's recommendations. Total RNA was
558 eluted in 30 µL of nuclease-free H_2O by centrifugation at 8,500 x g for 1 min at 4°C. To
559 overcome the confounding effect of heparin on qPCR[31,32], RNA was treated with heparinase
560 as described previously[33]. Briefly, 8 µL of RNA was added to 2 µL of heparinase 1 from
561 Flavobacterium (Sigma, H2519), 0.4 µL RNase inhibitor (Ribo Lock 40U/µL, ThermoFisher,
562 EO0381) and 5.6 µL of heparinase buffer (pH 7.5) and incubated at 25°C for 3 h.
563
564 **Reverse transcription-quantitative polymerase chain reaction (RT-qPCR).** For detection
565 of SARS-CoV-2 RNA we performed a two-step RT-qPCR using the LunaScript® RT
566 SuperMix Kit (NEB, E3010) and the Luna Universal Probe qPCR Master Mix (NEB, M3004)

567 according to the manufacturer's recommendations, apart from reducing the total qPCR reaction
568 volume to 5 μL and loading a cDNA dilution of 1:4 instead of 1:8 when performing the qPCR
569 reaction. Primer/probe sequences targeting the SARS-CoV-2 nucleocapsid (N) gene (N1 and
570 N2) were predesigned by Integrated DNA Technologies (IDT, 10006821, 10006822,
571 10006823, 10006824, 10006825, 10006826) according to the protocol for the detection of
572 SARS-CoV-2 of the United States Centers for Disease Control and Prevention (US CDC),
573 using 5' FAM / ZEN™ / 3' Iowa Black™ FQ probes. The qPCR reaction concentration for
574 probe (125 nM), forward (500 nM) and reverse primers (500 nM) were used according to the
575 US CDC protocol. A plasmid positive control (2019-nCoV_N Positive Control plasmid, IDT,
576 10006625) was measured on each qPCR plate. Reactions were loaded using a Bravo
577 Automated Liquid Handling Platform (Agilent). qPCR was performed on a ViiA7 Real-Time
578 PCR System (Applied Biosystems). Samples were considered positive for SARS-CoV-2 if the
579 cycle quantification (Cq) value of either N1 or N2 was below 40. Abundance of SARS-CoV-2
580 RNA in patients who tested positive had a mean Cq of 34.4; range: 29.8-37.6. As reported
581 before[73], N1 primers returned lower Cq values (higher abundance) than N2 primers
582 (Supplementary Fig. 7).
583
584 **Measurement of anti-SARS-CoV-2 antibodies.** IgG antibodies against the SARS-CoV-2
585 spike S1 domain were measured by ELISA (Anti-SARS-CoV-2 IgG ELISA, Euroimmun, EI
586 2606-9601 G) according to the manufacturer's recommendations. Since no international
587 reference serum for anti-SARS-CoV-2 antibodies exists, calibration was performed in ratios,
588 giving relative antibody quantification. Neutralizing antibodies against SARS-CoV-2 were
589 measured using a Surrogate Virus Neutralization Test (SARS-CoV-2 sVNT Kit, GenScript,
590 L00847) according to the manufacturer's recommendations. This ELISA-based kit detects
591 antibodies that are able to block the interaction between the SARS-CoV-2 spike receptor

592 binding domain (RBD) and the angiotensin converting enzyme (ACE2) cell receptor. For
593 validation of sVNT measurements in a subset of samples, neutralization potency was measured
594 using HIV-1 (human immunodeficiency virus-1) based virus particles, pseudotyped with
595 SARS-CoV-2 spike protein in a HeLA cell line stably expressing the ACE2 receptor, as
596 described previously[13].
597
598 **In-solution protein digestion.** 10 µL of inactivated serum or plasma were denatured by the
599 addition of urea (final concentration 7.2 M) and reduced using dithiothreitol (final
600 concentration 5 mM) for 1 h at 37 °C and 180 rpm. Reduced proteins were cooled down to
601 room temperature before being alkylated in the dark for 1 h using iodoacetamide (final
602 concentration 25 mM). An aliquot equivalent to 40 µg of alkylated protein was added to a
603 0.1 M triethylammonium bicarbonate solution (pH 8.2) and digested for 18 h at 37 °C, at
604 180 rpm using 1.6 µg of Trypsin/LysC (Promega, V5072). Digested peptide solutions were
605 acidified using trifluoroacetic acid (TFA, final concentration 1 %).
606
607 **Peptide clean-up and stable isotope-labelled standard (SIS) spike-in.** Peptide clean-up was
608 achieved using a Bravo AssayMAP Liquid Handling Platform (Agilent). After conditioning
609 and equilibration of the resin, acidified peptide solutions were loaded onto AssayMAP C18
610 Cartridges (Agilent, 5190-6532), washed using 1 % acetonitrile (ACN), 0.1 % TFA (aq) and
611 eluted using 70 % ACN, 0.1 % TFA (aq). Eluted peptides were vacuum centrifuged (Thermo
612 Scientific, Savant SPD131DDA) to dry and resuspended in 40 µL of 2 % ACN, 0.05 % TFA
613 (aq). For clinical cohort analysis, 6 µL of cleaned peptide solution was added to two injection
614 equivalents of PQ500 SIS mix (Biognosys) using a Bravo Liquid Handling Platform (Agilent).
615

616 **Data-independent acquisition-mass spectrometry (DIA-MS) analysis.** Peptides were
617 analyzed using a high-performance liquid chromatography (HPLC)-MS assembly consisting
618 of an UltiMate 3000 HPLC system (Thermo Scientific) which was equipped with a capillary
619 flow selector and coupled via an EASY-Spray NG Source (Thermo Scientific) to an Orbitrap
620 Fusion Lumos Tribrid mass spectrometer (Thermo Scientific). To generate DIA data for serum
621 samples (GSTT COVID-19 ICU cohort) and plasma samples (KCH COVID-19 ICU cohort,
622 the pre-pandemic sepsis ICU cohort and the pre-pandemic control patients before elective
623 cardiac surgery), peptides were injected onto a C18 trap cartridge (Thermo Scientific, 160454)
624 at a flow rate of 25 µL / min for 1 min, using 0.1% formic acid (FA, aq). The initial capillary
625 flow rate was reduced from 3 to 1.2 µL / min in 1 min at 1% B. Peptides were then eluted from
626 the trap cartridge and separated on an analytical column (Thermo Scientific, ES806A, at 50
627 °C) using the following gradient: 1–11 min, 1–5% B; 11–32 min, 5–18% B; 32–52 min, 18–
628 40% B; 52–52.1 min, 40–99% B; 52.1–58 min, 99% B. The flow rate was increased to
629 3 µL/min and the column was washed using the following gradient: 58–58.1 min, 99–1% B;
630 58.1–59.9 min, 1–99% B; 59.9–60 min, 99–1% B. Finally, the column was equilibrated at 1%
631 B for 6 min. In all HPLC-DIA-MS analyses, mobile phase A was 0.1% FA (aq) and mobile
632 phase B was 80% ACN, 0.1% FA (aq). Precursor MS1 spectra were acquired using Orbitrap
633 detection (resolution 60000 at 200 m/z, scan range 329–1201 m/z). Quadrupole isolation was
634 used to sequentially scan 30 precursor m/z windows of variable width (Supplementary Table
635 10). Per isolation window, semi-targeted Orbitrap MS2 spectra (resolution 30000 at 200 m/z)
636 were collected following higher-energy C-trap dissociation.
637
638 **MS database search for DIA-MS analysis.** PQ500 SIS-spiked DIA data from all serum and
639 plasma samples of the GSTT COVID-19 ICU cohort, the KCH COVID-19 ICU cohort, the
640 non-COVID-19 sepsis ICU cohort and the control patients before elective cardiac surgery were

641 analyzed in Spectronaut v14 (Biognosys AG), using the provided PQ500 analysis plug-in. MS1
642 and MS2 mass tolerance strategies were set to relative at a tolerance of 20 ppm, while MS2
643 mass tolerance was set to dynamic. Retention time calibration was achieved using the spiked
644 iRT peptides included in the PQ500 SIS mix. Precursor and protein Q-value cutoff was set to
645 0.01. Quantification was conducted at an MS2 level using peak areas and individual runs were
646 normalized using the global strategy set to median. All peptides for reported proteins were
647 manually checked to ensure accurate peak integration across all samples. Peptides with a Q-
648 value of more than 0.01 or a signal to noise ratio of less than 5 were marked as missing. Peptides
649 with more than 30% missing values across all samples were filtered out and the remaining
650 missing values were imputed using the KNN algorithm (K = 5)[74]. Spearman correlations of
651 peptides belonging to the same protein were computed. In case more than two peptides per
652 protein were detected, peptides were filtered if their correlation with the remaining peptides
653 was less than r = 0.4. In case two peptides per protein were detected, the most abundant peptide
654 was kept even when correlation was less than r = 0.4. Final protein abundance was calculated
655 by summing up the quantified peptide abundances. Final quantitative comparisons were
656 conducted using the light/heavy peptide abundance ratio. For validation of our DIA-MS data,
657 we correlated levels to clinical measurements of albumin (n = 49, r = 0.68, P <0.05) and C-
658 reactive protein (n = 49, r = 0.83, P <0.05) as examples of high and medium-abundant proteins.
659

660 **SARS-CoV-2 spike protein pull-down**. His-tagged recombinant SARS-CoV-2 spike
661 glycoprotein (RP-87680, ThermoFisher) was added to 1:2 PBS-diluted plasma from COVID-
662 19 ICU patients (n = 8) or non-COVID-19 controls (n = 3) at 200 ng/µL and incubated
663 overnight at 4°C with intermittent mixing. His-tagged spike was then isolated by means of
664 metal affinity magnetic beads (Dynabeads His-Tag Isolation and Pull-down, 10103D,
665 ThermoFisher) and eluted in imidazole-containing phosphate buffer. Proteins in the pull-down

666 isolates were denatured, reduced, alkylated and precipitated, as described above. Proteins
667 interacting non-specifically with the solid phase were determined by incubating plasma
668 samples with magnetic beads without the addition of His-tagged spike. Pull-down of His-
669 tagged spike without addition of plasma was performed as an additional control. Spike pull-
670 down protein digestion followed the same protocol outlined above.
671
672 **Data-dependent acquisition (DDA)-MS analysis.** Proteins from the spike pull-down
673 experiments were subject to in-solution tryptic digestion and C18 cleanup as described above.
674 Tryptic peptides were analyzed by LC-MS/MS. An UltiMate 3000 HPLC system (Thermo
675 Scientific) with a nanoflow selector was coupled via an EASY-Spray Source (Thermo
676 Scientific) to a Q Exactive HF mass spectrometer (Thermo Scientific). Peptides were injected
677 onto a C18 trap cartridge (Thermo Scientific, 160454) at a flow rate of 25 µL / min for 1 min,
678 using 0.1% FA (aq). Peptides were eluted from the trap cartridge and separated on an analytical
679 column (EASY-Spray C18 column, 75 µm x 50 cm, Thermo Scientific, ES803A, at 45 °C) at
680 a flow rate of 0.25 µL / min using the following gradient: 0–1 min, 1% B; 1–6 min, 1–6% B;
681 6−40 min, 6−18% B; 40–70 min, 18–35% B; 70–80 min, 35–45% B; 80–81 min, 45–99% B;
682 81–89.8 min, 99% B; 89.8–90 min, 99–1% B; 90–120 min, 1% B. Mobile phase A was 0.1%
683 FA (aq) and mobile phase B was 80% ACN, 0.1% FA (aq). Precursor MS1 spectra were
684 acquired using Orbitrap detection (resolution 60000 at 200 m/z, scan range 350–1600). Data-
685 dependent MS2 spectra of the most abundant precursor ions were obtained after higher-energy
686 C-trap dissociation and Orbitrap detection (resolution 15000 at 200 m/z) with TopN mode
687 (loop count 15) and dynamic exclusion (duration 40 s) enabled.
688
689 **MS database search for DDA-MS analysis**. Proteome Discoverer software (version
690 2.3.0.523, Thermo Scientific) was used to search raw SARS-CoV-2 spike glycoprotein pull-

691 down data files against a human database (UniProtKB/Swiss-Prot version 2020 01, 20,365
692 protein entries) supplemented with SARS-CoV-2 spike glycoprotein (1 protein entry) using
693 Mascot (version 2.6.0, Matrix Science). The mass tolerance was set at 10 ppm for precursor
694 ions and 0.02 Da for fragment ions. Trypsin was used as the digestion enzyme with up to two
695 missed cleavages being allowed. Carbamidomethylation of cysteines and oxidation of
696 methionine residues were chosen as fixed and variable modifications, respectively.
697
698 **Machine learning**. In addition to statistical techniques, machine learning was deployed to
699 identify a prognostic classifier for COVID-19 ICU patients based on 27 clinical variables,
700 RNAemia and three ELISA measurements. The RNAemia feature was defined as a binary
701 feature which takes a true value when RNAemia was present within six days upon admission
702 to ICU. Statistical significance with P value <0.05 was used as selection criterium for singleton
703 markers. The shortlisted singleton markers were subsequently compared in binary and triplet
704 combinations with all 27 clinical variables, RNAemia and the three ELISA measurements of
705 PTX3, RAGE and LGALS3BP. In this setup, binary and triplet combinatorial feature search
706 was performed using wrapper feature selection[75] with support vector machine (SVM) classifier
707 using radial basis function (RBF) kernel. Feature combinations were evaluated using the
708 average of sensitivity, positive predicted value (PPV) and area under the receiver operating
709 characteristic curve (ROC AUC) metrics. Given the imbalanced data with positive class *i.e.*
710 non-survivors as the minority class, PPV along with sensitivity helps to balance false positives
711 and false negatives. Combined with ROC AUC, it further facilitates equilibrium between
712 sensitivity and specificity with high prediction probability. SVM uses hyperplane (decision
713 surface) leveraging only a percentage of training samples (support vectors), thus offering high
714 generalization ability attributed to its near impervious characteristic to new samples[76].
715 Combinations were restricted to a maximum of triplets to enhance ease of clinical

716 implementation and avoid the risk of overfitting. Additionally, 10-fold cross validation along
717 with leave-one-out validation was used to avoid overfitting and test model generalization. The
718 SVM Synthetic Minority Oversampling Technique (SMOTE) was used to prevent learning bias
719 of SVM RBF towards the majority class[77]. Tuning of SVM RBF external parameter *i.e.* C was
720 performed using grid search. The Scikit-learn default *i.e.* 'scale' was used for the SVM RBF
721 gamma parameter[78]. A permutation test was performed to evaluate the null hypothesis that the
722 classifier performance is by chance *i.e.* input variables and outcome labels are independent[79].
723 Hence, rejection of the null hypothesis implies that the classifier has found a real class structure
724 (pattern) in the data. For technical validation of our 'Age, RNAemia' model based on SVM
725 RBF, we employed a permutation test for statistical significance of the classifier performance;
726 and stability of feature importance in an alternate machine learning feature ranking model *i.e.*
727 Random forest with resampling. Age and RNAemia were ranked among the top five most
728 important features based on mean importance across 100 resampling cycles of sensitivity
729 analysis. A permutation test with 50 permutes *i.e.* repeating the classification procedure after
730 random permuting of the outcome labels returned a significant *P* value (Supplementary Fig.
731 8). The implementation of machine learning was done using Scikit-learn 0.23.2 python
732 package[78].
733
734 **Statistical analysis**. Mann-Whitney U significance test was used for continuous variables and
735 Fisher exact test for binary variables. Spike pull-down data was analyzed by paired or unpaired
736 Student's t-tests as appropriate. Statistical comparisons on MS data were performed using the
737 Ebayes algorithm of the limma package correcting for age and sex. Timepoint comparisons
738 were performed using the non-parametric Kruskal Wallis test. Correlation patterns between
739 continuous variables were analyzed using Spearman correlation. Correlation between
740 categorical and continuous variables was examined using point-biserial correlation[80]. Anti-

741 SARS-CoV-2 antibody data and trajectories of protein clusters were fitted using Generalized
742 Alternative Models (GAM), with *P* values reporting the effect of RNAemia or mortality in the
743 model. Survival analysis was performed using Cox regression and Kaplan-Meier plots
744 leveraging the R 'survival' package. All features were scaled to a mean of zero and a standard
745 deviation of one. Features with missing values ≥30% were dropped and not used for data
746 analysis. This resulted in two clinical variables being dropped, *i.e.* eosinophils and basophils.
747 The remaining features were imputed, as applicable, using K nearest neighbors (KNN) based
748 imputation with $K = 5$ (Supplementary Table 11)[74]. To validate DIA-MS findings a publicly
749 available proximity-extension assay proteomics-based dataset was analyzed *(Data provided by*
750 *the MGH Emergency Department COVID-19 Cohort (Filbin, Goldberg, Hacohen) with Olink*
751 *Proteomics*). Differential expression analysis of proteins in survivors and non-survivors 28-
752 days after hospitalization within the Olink dataset was achieved through the Ebayes method of
753 the limma package. Statistical analysis and associated Figures were generated with R
754 programming environment (version 4.02), Python programming environment (version 3.8.6)
755 and GraphPad software (version 8.4.3). Schematic diagrams were created with Biorender.com.
756

Acknowledgements

M.M. and A.M.S. are British Heart Foundation (BHF) Chair Holders with BHF program grant support (CH/16/3/32406, RG/16/14/32397 and CH/1999001/11735, RE/18/2/34213, respectively). C.G., E.R. and B.S. are funded by BHF PhD studentships (FS/18/60/34181, FS/17/65/33481, FS/19/58/34895). M.H. is funded by an interdisciplinary PhD studentship from King's BHF Centre of Research Excellence. M.F. is funded by a National Institute of Academic Anesthesia BJA-RCOA PhD Fellowship WKR0-2018-0047. M.J.W.M. is grateful to the Biomedical Research Centre at Guy's and St Thomas' NHS Foundation Trust for support. K.O.G. is supported by a UK Medical Research Council Clinical Research Training Fellowship (MR/R017751/1). K.J.D was supported by a King's Together Rapid COVID-19 Call award, by an MRC Discovery Award (MC/PC/15068), Huo Family Foundation and the Fondation Dormeur, Vaduz. The NIHR Collaboration for Leadership in Applied Health Research and Care South London at King's College Hospital NHS Foundation Trust, awarded to J.D.E. who is also supported by a charitable donation from the Lower Green Foundation.

M.M.'s research was made possible through the support of the BIRAX Ageing Initiative and funding from the EU Horizon 2020 research and innovation program under the Marie Skłodowska-Curie grant agreement No 813716 (TRAIN-HEART), the Leducq Foundation (18CVD02), the excellence initiative VASCage (Centre for Promoting Vascular Health in the Ageing Community, project number 868624) of the Austrian Research Promotion Agency FFG (COMET program–Competence Centers for Excellent Technologies) funded by the Austrian Ministry for Transport, Innovation and Technology; the Austrian Ministry for Digital and Economic Affairs; and the federal states Tyrol (via Standortagentur), Salzburg, and Vienna (via Vienna Business Agency), two BHF project grant supports (PG/17/48/32956, SP/17/10/33219) and the BHF Centre for Vascular Regeneration with Edinburgh/Bristol (RM/17/3/33381). M.M. and S.R.B. acknowledge support as visiting professors as part of the

Transcampus TU Dresden King's College London Initiative. The work of A.C.H. is supported by a Cancer ImmunoTherapy Accelerator award from CRUK; the Wellcome Trust (106292/Z/14/Z); the Rosetrees Trust; King's Together Seed Fund; The John Black Charitable Foundation; Royal Society Grant IES\R3\170319 and the Francis Crick Institute, which receives core funding from Cancer Research UK (FC001093), the MRC (FC001093) and the Wellcome Trust (FC001093). M.S.H. is supported by the National Institute for Health Research Clinician Scientist Award (CS-2016-16-011). The research was funded/supported by the National Institute for Health Research (NIHR) Biomedical Research Centre based at Guy's and St Thomas' NHS Foundation Trust and King's College London. The views expressed are those of the author(s) and not necessarily those of the NHS, the NIHR or the Department of Health.

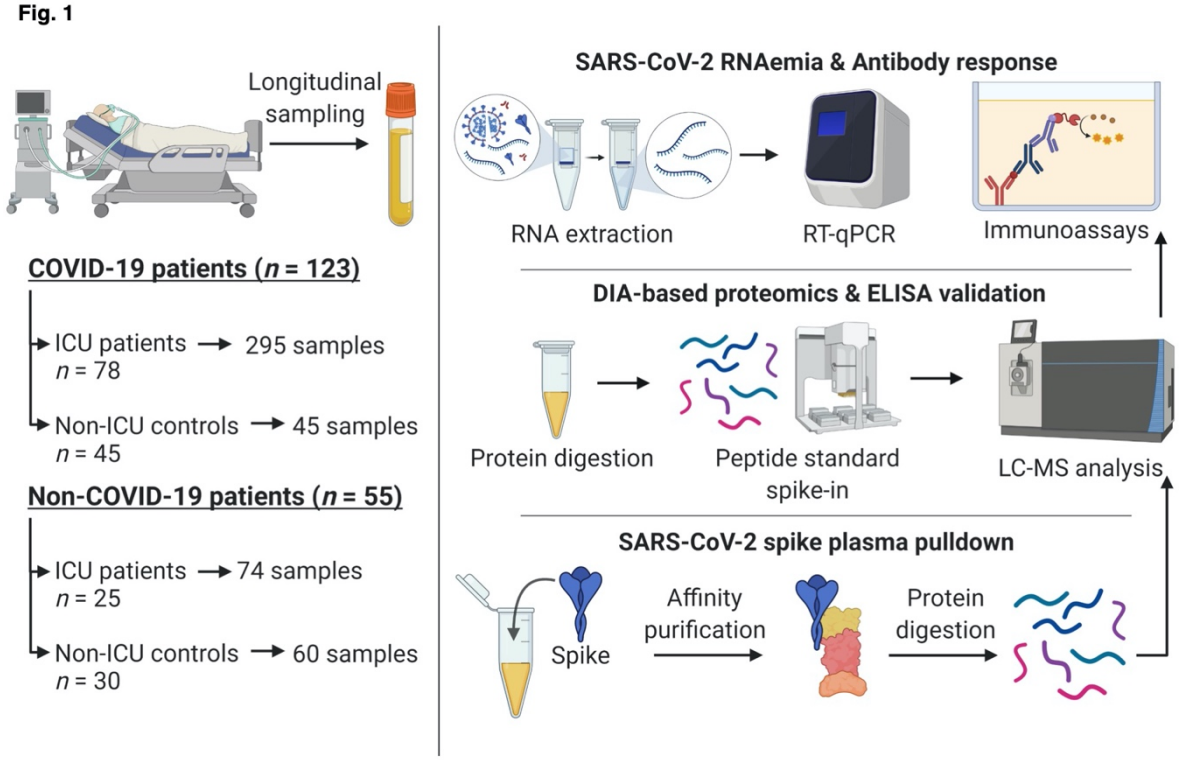

Fig. 1. Schematic of study design. Plasma and serum samples were obtained from multiple patient cohorts across two UK-based university hospitals, including 123 COVID-19 patients: 78 SARS-CoV-2 positive patients in ICU were sampled at multiple time points over a 2-week period and compared to hospitalized non-ICU SARS-CoV-2 positive patients (n = 45). We used non-COVID-19 ICU patients (n = 25) and patients before and after undergoing elective cardiac surgery (n = 30) as controls. Patient samples were assessed for SARS-CoV-2 RNAemia, antibody responses and protein changes in the circulation. Finally, plasma protein interactions with SARS-CoV-2 spike glycoprotein were determined using a pull-down assay followed by mass spectrometry analysis.

Fig. 2

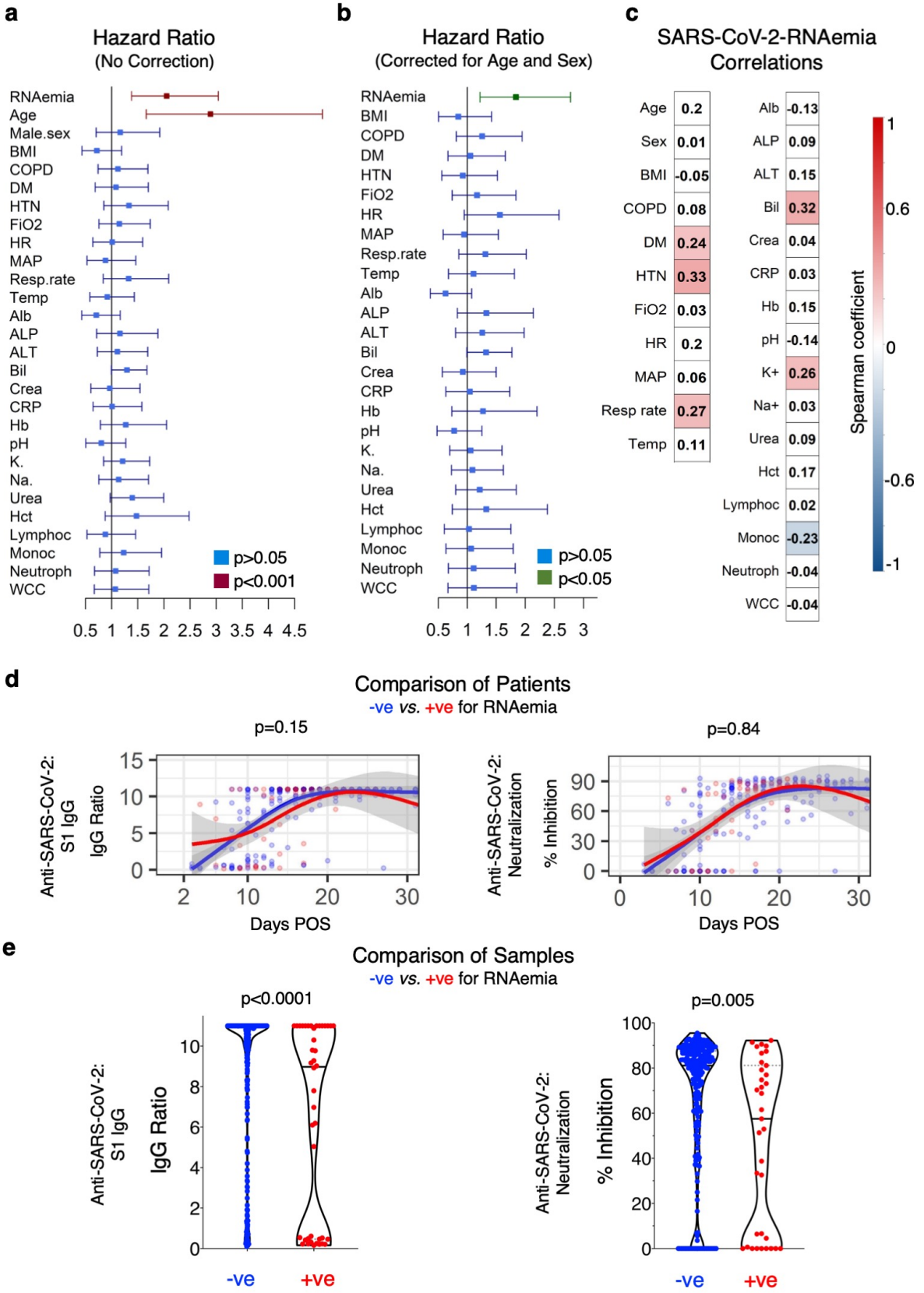
a
Hazard Ratio
(No Correction)
RNAemia
Age
Male.sex
BMI
COPD
DM
HTN
FiO2
HR
MAP
Resp.rate
Temp
Alb
ALP
ALT
Bil
Crea
CRP
Hb
pH
K.
Na.
Urea
Hct
Lymphoc
Monoc
Neutroph
WCC
p>0.05
p<0.001
0.5 1 1.5 2 2.5 3 3.5 4 4.5
b
Hazard Ratio
(Corrected for Age and Sex)
RNAemia
BMI
COPD
DM
HTN
FiO2
HR
MAP
Resp.rate
Temp
Alb
ALP
ALT
Bil
Crea
CRP
Hb
pH
K.
Na.
Urea
Hct
Lymphoc
Monoc
Neutroph
WCC
p>0.05
p<0.05
0.5 1 1.5 2 2.5 3
c
SARS-CoV-2-RNAemia
Correlations
Age 0.2
Sex 0.01
BMI -0.05
COPD 0.08
DM 0.24
HTN 0.33
FiO2 0.03
HR 0.2
MAP 0.06
Resp rate 0.27
Temp 0.11
Alb -0.13
ALP 0.09
ALT 0.15
Bil 0.32
Crea 0.04
CRP 0.03
Hb 0.15
pH -0.14
K+ 0.26
Na+ 0.03
Urea 0.09
Hct 0.17
Lymphoc 0.02
Monoc -0.23
Neutroph -0.04
WCC -0.04
Spearman coefficient
1
0.6
0
-0.6
-1
d
Comparison of Patients
-ve vs. +ve for RNAemia
p=0.15
Anti-SARS-CoV-2: S1 IgG
IgG Ratio
15
10
5
0
2 10 20 30
Days POS
p=0.84
Anti-SARS-CoV-2: Neutralization
% Inhibition
90
60
30
0
0 10 20 30
Days POS
e
Comparison of Samples
-ve vs. +ve for RNAemia
p<0.0001
Anti-SARS-CoV-2: S1 IgG
IgG Ratio
10
8
6
4
2
0
-ve
+ve
p=0.005
Anti-SARS-CoV-2: Neutralization
% Inhibition
100
80
60
40
20
0
-ve
+ve

803

804 **Fig. 2. SARS-CoV-2 RNAemia and the humoral immune response. a**, Unadjusted hazard ratios
805 based on two ICU patient cohorts (KCH and GSTT, 60 survivors and 18 non-survivors). Green indicates
806 *P* value <0.05, maroon indicates *P* value <0.001 and blue indicates *P* value >0.05. **b**, Hazard ratios after
807 adjustment for age and sex. **c**, Association of SARS-CoV-2 RNAemia with binary variables (Spearman
808 correlation) and continuous variables (point-biserial correlation). Red indicates positive and blue
809 negative correlation with *P* value <0.05. Abbreviations: Alb: albumin, ALP: alkaline phosphatase, ALT:
810 alanine aminotransferase, Bil: bilirubin, COPD: Chronic obstructive pulmonary disease, Crea:
811 Creatinine, CRP: C-reactive protein, DM: Diabetes, Hct: Hematocrit, Hb: Hemoglobin, HR: Heart rate,
812 HTN: Hypertension, Lymphoc: Lymphocytes, MAP: Mean arterial pressure, Monoc: Monocytes,
813 Neutroph: Neutrophils, K^+: Potassium, Resp. rate: Respiratory rate, Na^+: Sodium, Temp: Body
814 temperature, WCC: White cell count. **d,** Anti-SARS-CoV-2 spike IgG and (**d**) anti-SARS-CoV-2
815 neutralization response (**d**) based on days post onset of symptoms (POS) in patients who tested positive
816 (red) or negative (blue) for plasma/serum SARS-CoV-2 RNA within the first six ICU days. Lines show
817 fitted Generalized Additive Models (GAM) with grey bands indicating the 95% interval of trust,
818 correcting for age and sex. **e**, Anti-SARS-CoV-2 spike IgG levels (**e**) and anti-SARS-CoV-2
819 neutralization capacity (**e**) in individual samples positive or negative for SARS-CoV-2 RNA.
820 Significance was determined through the Mann-Whitney U test. *P* values are corrected for age, sex and
821 days POS.

822

Fig. 3

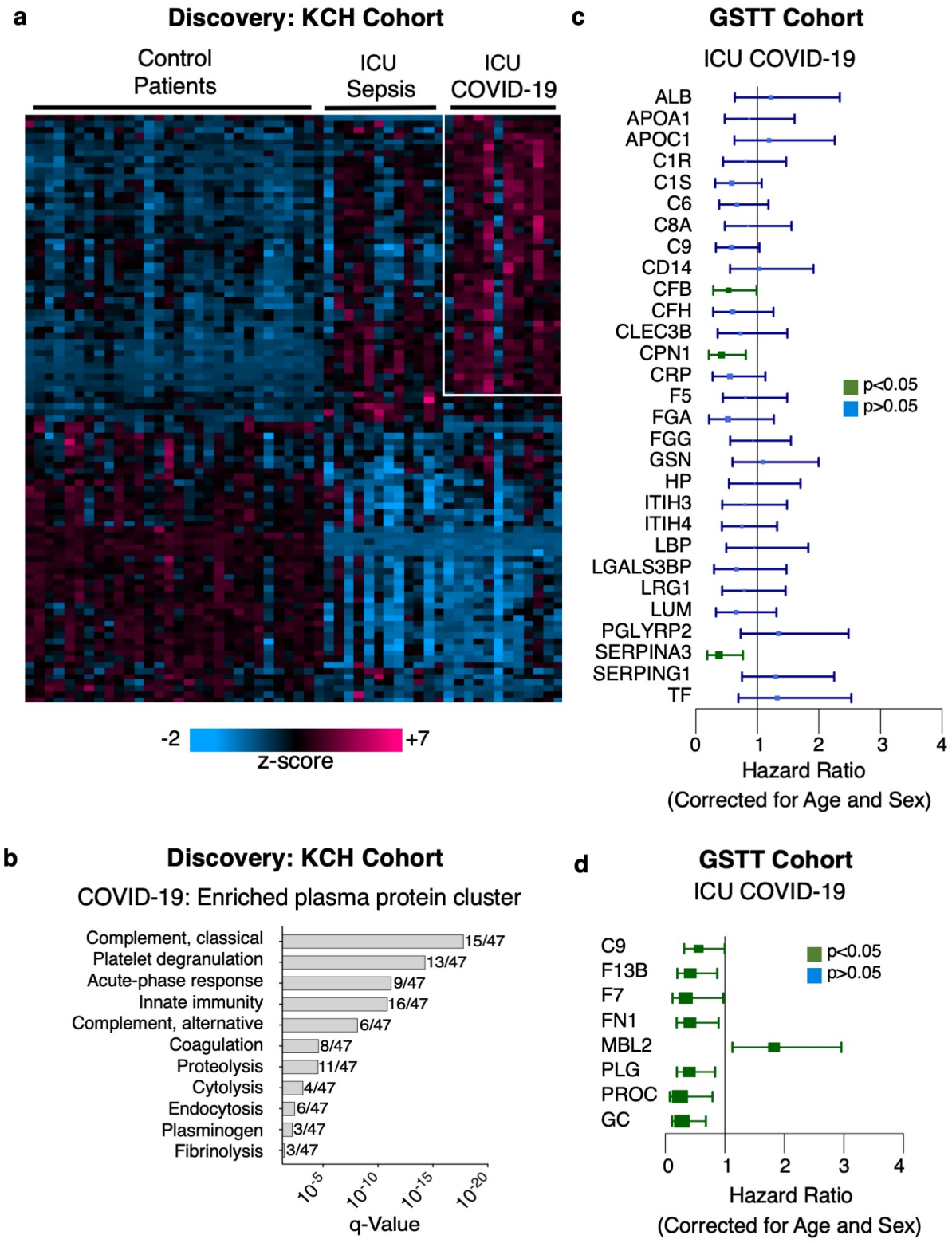
a
Discovery: KCH Cohort
Control Patients
ICU Sepsis
ICU COVID-19
-2
+7
z-score
c
GSTT Cohort
ICU COVID-19
ALB
APOA1
APOC1
C1R
C1S
C6
C8A
C9
CD14
CFB
CFH
CLEC3B
CPN1
CRP
F5
FGA
FGG
GSN
HP
ITIH3
ITIH4
LBP
LGALS3BP
LRG1
LUM
PGLYRP2
SERPINA3
SERPING1
TF
p<0.05
p>0.05
0
1
2
3
4
Hazard Ratio
(Corrected for Age and Sex)
b
Discovery: KCH Cohort
COVID-19: Enriched plasma protein cluster
Complement, classical
Platelet degranulation
Acute-phase response
Innate immunity
Complement, alternative
Coagulation
Proteolysis
Cytolysis
Endocytosis
Plasminogen
Fibrinolysis
15/47
13/47
9/47
16/47
6/47
8/47
11/47
4/47
6/47
3/47
3/47
10-5
10-10
10-15
10-20
q-Value
d
GSTT Cohort
ICU COVID-19
C9
F13B
F7
FN1
MBL2
PLG
PROC
GC
p<0.05
p>0.05
0
1
2
3
4
Hazard Ratio
(Corrected for Age and Sex)

823

824 **Fig. 3. COVID-19 circulating proteome signature and associations with 28-day mortality. a**,
825 Plasma proteome profiling was conducted using a data-independent acquisition-mass spectrometry
826 (DIA-MS) approach with spiked standards for 500 proteins. Hierarchical cluster analysis was conducted
827 upon significantly changing plasma proteins across control patients before elective cardiac surgery (*n* =
828 30), ICU patients with sepsis (*n* = 12) and ICU patients with COVID-19 (*n* = 12, KCH). The heatmap
829 highlights 47 proteins enriched in COVID-19. Kruskal-Wallis, BH correction $q<0.05$. **b**, Gene ontology
830 enrichment analysis was conducted upon these 47 proteins and significantly enriched pathways are
831 represented. **c**, 29 common proteins cross-referenced against two published proteomic studies, exploring
832 protein biomarkers of COVID-19 severity. The ability of these 29 proteins to predict 28-day mortality
833 was explored in an independent ICU patient cohort (GSTT) by DIA-MS, and hazard ratio plots are
834 shown. **d**, Proteomic analysis by DIA-MS conducted upon the serum samples of the GSTT COVID-19
835 ICU cohort returned additional biomarker candidates that predict 28-day mortality. Significance was
836 determined through the Kruskal-Wallis test with Benjamini and Hochberg's FDR correction.

837

Fig. 4

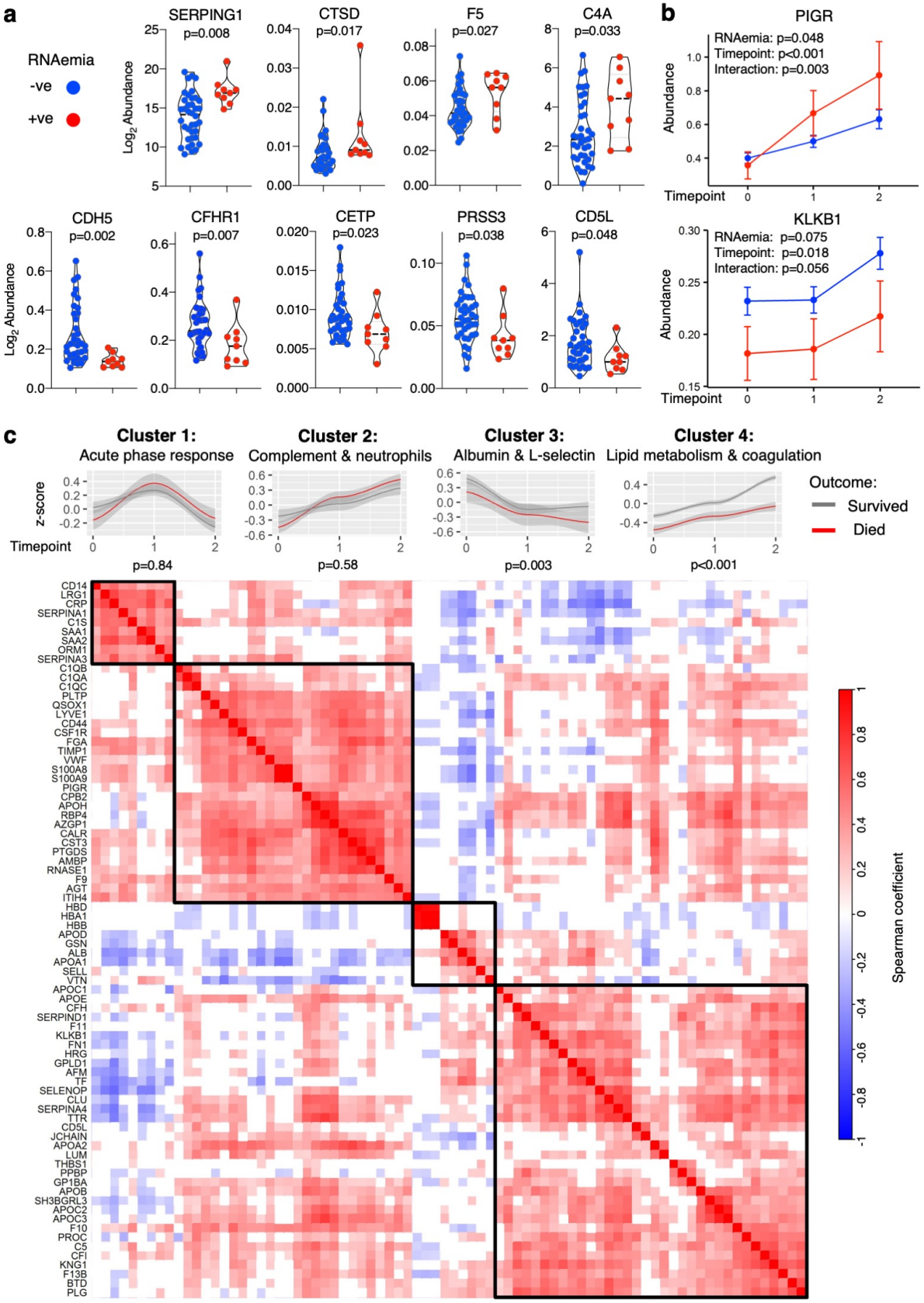
a
RNAemia
-ve
+ve
SERPING1
p=0.008
CTSD
p=0.017
F5
p=0.027
C4A
p=0.033
CDH5
p=0.002
CFHR1
p=0.007
CETP
p=0.023
PRSS3
p=0.038
CD5L
p=0.048
Log2 Abundance
b
PIGR
RNAemia: p=0.048
Timepoint: p<0.001
Interaction: p=0.003
KLKB1
RNAemia: p=0.075
Timepoint: p=0.018
Interaction: p=0.056
Abundance
Timepoint
c
Cluster 1:
Acute phase response
Cluster 2:
Complement & neutrophils
Cluster 3:
Albumin & L-selectin
Cluster 4:
Lipid metabolism & coagulation
z-score
Timepoint
p=0.84
p=0.58
p=0.003
p<0.001
Outcome:
Survived
Died
Spearman coefficient

838

839 **Fig. 4. Circulating protein changes associated with SARS-CoV-2 RNAemia status over time. a**,
840 DIA-MS analysis upon serum samples from the GSTT COVID-19 ICU cohort was used to determine
841 proteins that associate with the presence of SARS-CoV-2 RNAemia. Proteins that were significantly
842 associated with RNAemia at baseline are individually represented as violin plots. Significance was
843 determined through the Limma linear model analysis using Benjamini and Hochberg's FDR correction.
844 Abbreviations: CDH5, cadherin-5 or VE-cadherin; CFHR1, complement factor H-related protein 1;
845 SERPING1, plasma protease C1 inhibitor; CTSD, cathepsin D; CETP, cholesteryl ester transfer protein;
846 F5, coagulation factor 5; C4A, complement factor 4a; PRSS3, trypsin-3; CD5a, CD5 antigen-like. **b**,
847 Proteins with significantly different trajectories over time (baseline, week 1 – time point 1, week 2 –
848 time point 2) between RNAemia positive and negative patients. PIGR, polymeric immunoglobulin
849 receptor; KLKB1, kallikrein B1. **c,** Serial serum samples from COVID-19 ICU patients (GSTT,
850 baseline, week 1 and week 2) were analyzed by DIA-MS to determine protein changes over time in
851 ICU. The heat map represents a hierarchical cluster analysis conducted upon a Spearman correlation
852 network of significantly changing proteins over time in ICU. Comparison of the trajectories of protein
853 clusters in COVID-19 ICU patients based on 28-day mortality. Gene ontology enrichment analysis was
854 used to determine functional pathways associated with the distinct protein clusters identified. Listed are
855 the protein clusters that show a significant change between 28-day survivors (grey) and non-survivors
856 (red) - and having a significant interaction with time points (baseline, week 1 – time point 1, week 2 –
857 time point 2). Lines show fitted Generalized Additive Models (GAM) with grey bands indicating the
858 95% interval of trust. *P* values represent the significance of the outcome term in a fitted GAM model
859 when correcting for age and sex.

860

Fig. 5

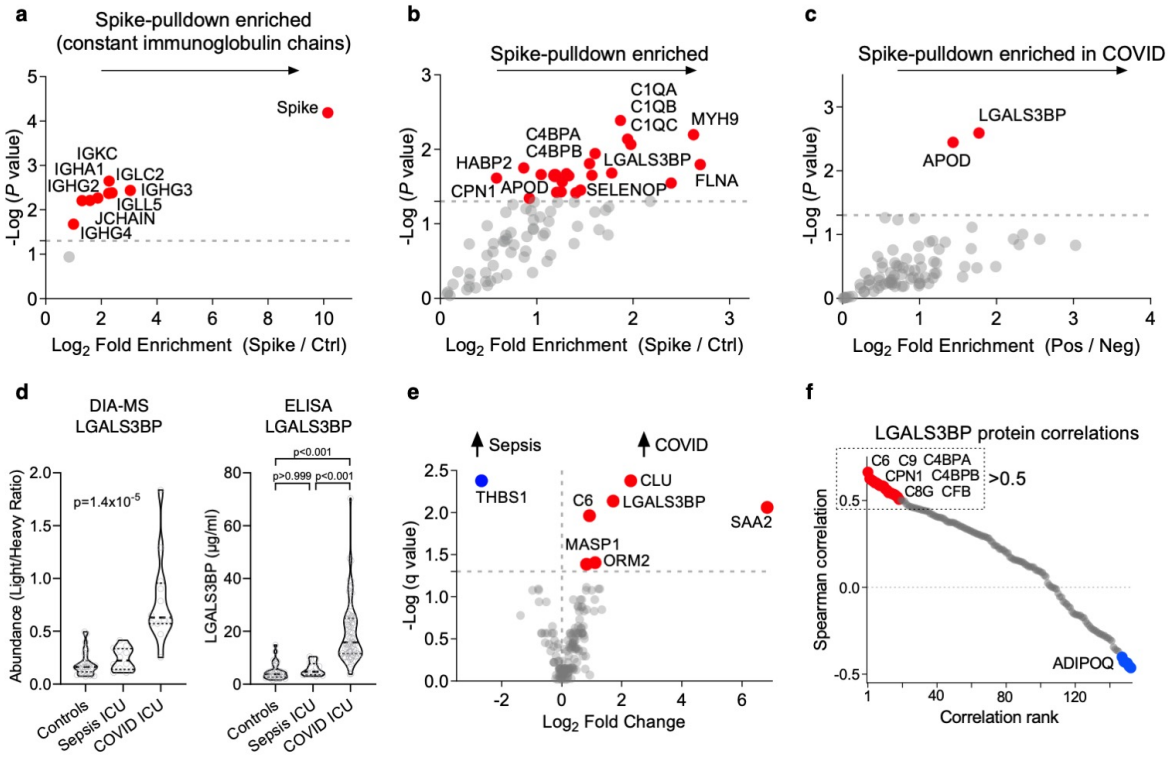

Fig. 5. LGALS3BP interacts with SARS-CoV-2 spike glycoprotein. a, Magnetic bead-based affinity isolation of binding partners using His-tagged SARS-CoV-2 spike glycoprotein as a bait for proteins in SARS-CoV-2-positive patient plasma. **b**, Volcano plot with significantly enriched proteins. **c**, Comparison of SARS-CoV-2 spike glycoprotein pull-down using plasma from COVID-19 ICU patients and non-COVID-19 sepsis ICU patients. Significance was determined by Student's t-test. **d,** LGALS3BP levels across three patient cohorts as determined by DIA-MS or ELISA: control patients before undergoing elective cardiac surgery (n = 30), pre-pandemic sepsis ICU patients (n = 12) and COVID-19 ICU patients (n = 74). Kruskal-Wallis and Dunn's multiple comparisons test were used to determine statistical significance. **e**, Volcano plot representing protein changes between baseline plasma samples from patients in ICU with either sepsis or COVID-19. Significance was determined through the Mann-Whitney U test with Benjamini and Hochberg's FDR correction. **f**, Plasma proteins correlating to LGALS3BP after age and sex corrections are highlighted by a Spearman correlation matrix across the proteomic dataset. Proteins with a Spearman correlation coefficient greater than 0.5 were used for Gene ontology pathway enrichment analysis (Supplementary Fig. 5).

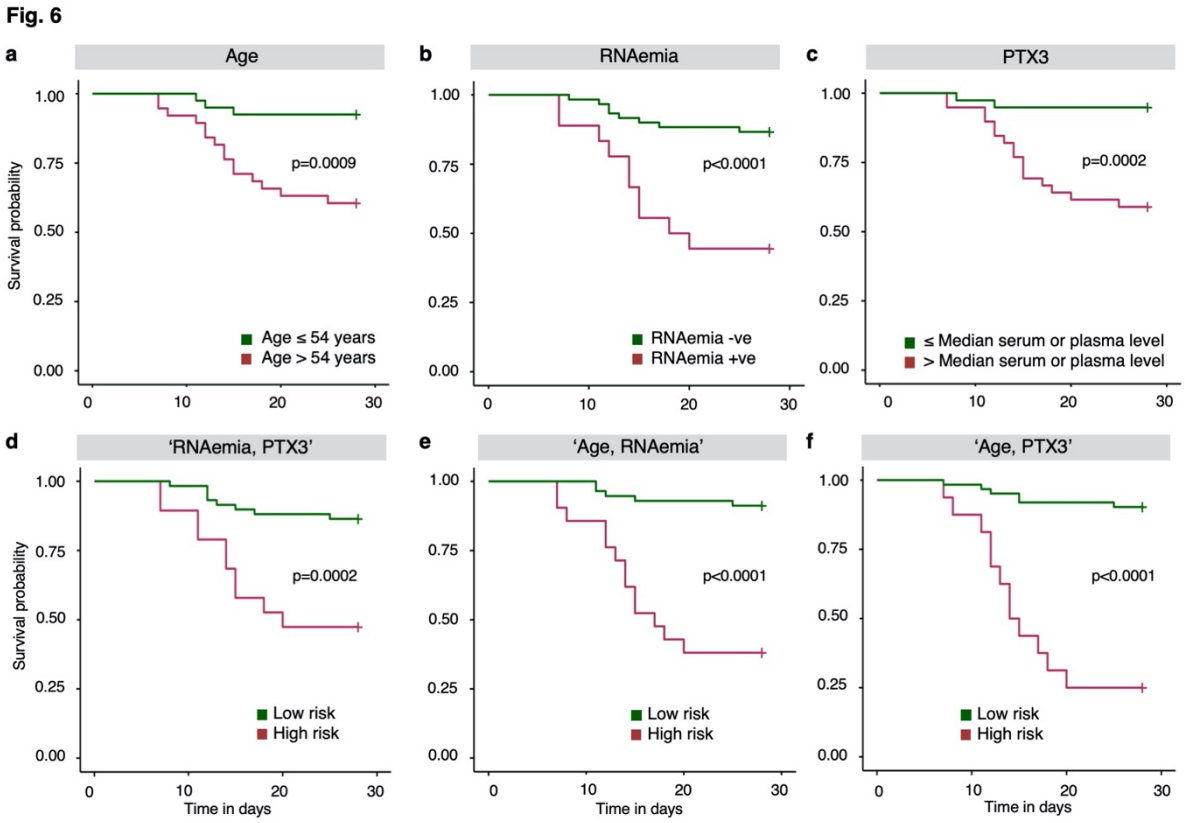

Fig. 6. SARS-CoV-2 mortality prediction using machine learning. **a**, Kaplan-Meier plot for age (using median age of 54 years). **b**, Kaplan-Meier plot for SARS-COV-2 RNAemia. As a single predictor, RNAemia provides the best stratification for survival. **c**, Kaplan-Meier plot for PTX3 using median of serum or plasma. **d, e, f**, Kaplan-Meier plots for 'RNAemia, PTX3', 'Age, RNAemia' and 'Age, PTX3' combined in SVM RBF machine learning model. The machine learning model selected binary combinations of 'Age, RNAemia' and 'Age, PTX3' as the best predictors.